



Cite this: *J. Mater. Chem. C*, 2016,
4, 468

Effect of intercalation and chromophore arrangement on the linear and nonlinear optical properties of model aminopyridine push–pull molecules[†]

Filip Bureš,^{*a} Daniel Cvejn,^a Klára Melánová,^b Ludvík Beneš,^c Jan Svoboda,^b Vítězslav Zima,^b Oldřich Pytela,^a Tomáš Mikyšek,^d Zdeňka Růžičková,^e I. V. Kityk,^f Artur Wojciechowski^f and Nasser AlZayed^f

Three push–pull aminopyridine derivatives having D–π–A, D–(π–A)₂, and D–(π–A)₃ arrangements were examined as model organic chromophores capable of intercalation into inorganic layered materials (alpha modification of zirconium hydrogen phosphate, zirconium 4-sulfophenylphosphonate, and gamma modification of titanium hydrogen phosphate). The fundamental properties of these dyes, their methylated analogues as well as their intercalates were studied by X-ray analysis, electrochemistry, UV/Vis absorption spectra, TGA, IR spectra, SHG, and were completed by DFT calculations. The synthesis of tripodal tris(pyridin-4-yl)amine is given for the first time. The HOMO–LUMO gap, the position of the longest-wavelength absorption maxima, and the dipole moment of aminopyridines can easily be tuned by attaching/removing pyridin-4-yl electron withdrawing units and their quaternization (pyridine vs. pyridinium acceptors). Their intercalation proved to be feasible affording novel inorganic–organic hybrid materials. The intercalation is accompanied by protonation of the guest, which enhances its ICT and strongly anchors the aminopyridines into the confined space of the layered host. Moreover, this process results in ordering of the organic chromophores and also brings improved thermal and chemical robustness. As a result, the measured SHG efficiencies of the intercalates are larger than those observed for the pure organic push–pull chromophores. Hence, the methodology of intercalation turned out to be very useful strategy for property tuning of NLO-active organic molecules.

Received 26th October 2015,
Accepted 1st December 2015

DOI: 10.1039/c5tc03499j

www.rsc.org/MaterialsC

Introduction

Owing to their easy and modular synthesis as well as peculiar properties such as distinct color, dipolar character, well-defined

and tunable structure, and supramolecular arrangement, organic push–pull molecules have become an extensively explored, and burgeoning area of organic and materials chemistry.¹ In such D–π–A systems direct intramolecular charge-transfer (ICT) from the electron donor (D) to the acceptor (A) takes place through the π-system and renders the molecule unique linear and nonlinear optical (NLO) properties. Hence, organic push–pull chromophores with large nonlinearities are of substantial interest for all-optical signal processing applications such as optical triggering, light frequency transducers, optical memories, modulators and deflectors.² On the molecular level, the rational design and property tuning in D–π–A systems rely mostly on modulation of the donating/withdrawing behavior of the D and A parts and extension of the π-system or production of D–π metal-ligand charge transfer complexes.^{1–3} At the same time, there exist fundamental limits for enhancement of the second-order hyperpolarizabilities of organic chromophores. These limits are mostly determined by energy of the transition from the ground to the first excited states and by the number of effective conjugated electrons.⁴ However and as a rule, enhanced hyperpolarizability decreases effective energy gap leading to lower transparency.

^a Institute of Organic Chemistry and Technology, Faculty of Chemical Technology, University of Pardubice, Studentská 573, Pardubice, 53210, Czech Republic.

E-mail: filip.bures@upce.cz

^b Institute of Macromolecular Chemistry, Academy of Science of the Czech Republic, Heyrovský sq. 2, 162 06 Prague 6, Czech Republic

^c Joint Laboratory of Solid State Chemistry, Faculty of Chemical Technology, University of Pardubice, 532 10 Pardubice, Czech Republic

^d Department of Analytical Chemistry, Faculty of Chemical Technology, University of Pardubice, 532 10 Pardubice, Czech Republic

^e Department of Inorganic and General Chemistry, Faculty of Chemical Technology, University of Pardubice, 532 10 Pardubice, Czech Republic

^f Electrical Engineering Department, Czestochowa University of Technology, Armii Krajowej 17, Czestochowa, 42201, Poland

† Electronic supplementary information (ESI) available: Synthesis of APY2–3, MeAPY1–3 and their intercalates, crystallographic data of APY3, structural analysis of MeAPY2, UV/Vis spectra in methanol, further DFT-calculated data, TGA curves, IR spectra, solid-state UV/Vis spectra, further NLO data. CCDC 1405923. For ESI and crystallographic data in CIF or other electronic format see DOI: 10.1039/c5tc03499j

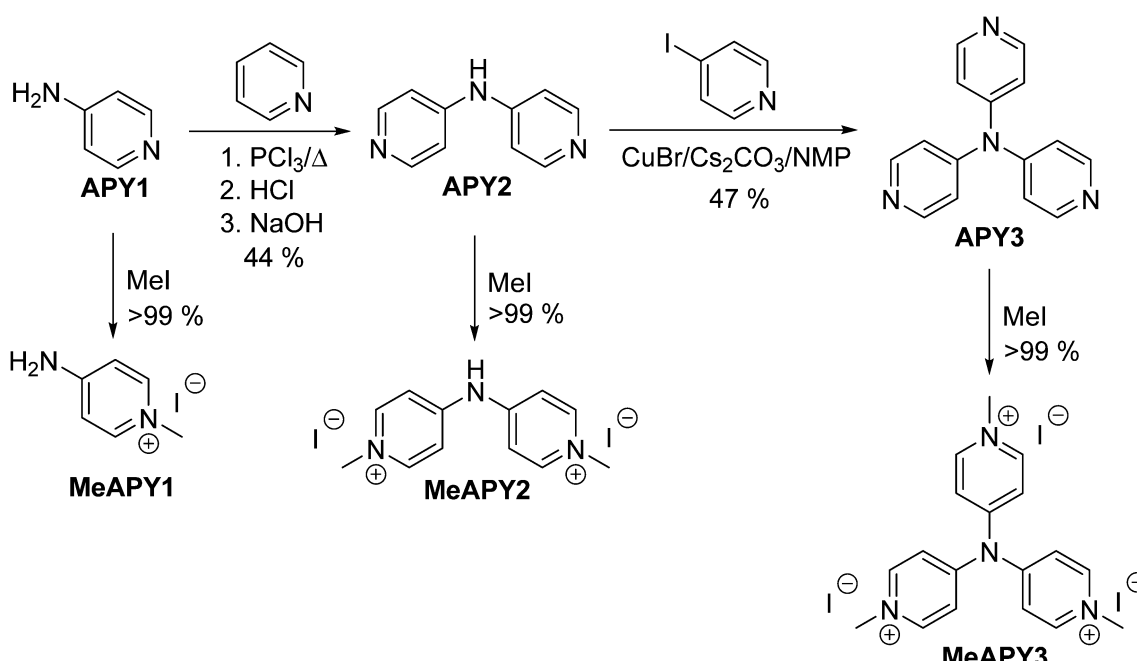


Based on such property tuning, admirable number of organic push-pull molecules with large intrinsic (hyper)polarizabilities were developed.⁵ However, it turned out to be rather difficult to translate their high molecular optical nonlinearity to macroscopic nonlinear- and electro-optic activity.⁶ The traditional approach to overcome this issue involves incorporation of the chromophore into a polymeric backbone (either covalently bound or doped), dendrimers, organic glasses, films as well as host-guest systems in which layered inorganic compounds might serve as the host matrix. The host matrix of the latter inorganic-organic hybrid systems comprises clays (LAPONITE[®], saponite, montmorillonite, hydrotalcite, kaoline *etc.*),⁷ silicates,⁸ and layered metal oxalates and MPS₃ (M = Mn, Cd, Zn).⁹ Formerly, organic NLOphores capable of intercalation were limited to simple and linear D- π -A systems such as nitroanilines or azobenzenes but, more recently, it was found that large heterocyclic molecules such as (di)azines, porphyrines and some branched chromophores undergo intercalation into a layered material as well.¹⁰ The incorporation of organic dyes into a restricted space of an ordered inorganic matrix represents important strategy for achieving materials with the following features and properties:

- the periodical ordering of the inorganic matrix, which can induce preferential orientation of the dye
- reduction of random 3D-orientation of the dye into a 2D-arrangement
- planarization of the π -system of the dye
- confined environment with reduced internal motion of the dye enhances its photophysical properties
- encapsulation of less stable organic molecules by a very robust and transparent inorganic carrier
- increased chemical and thermal stability.

Hence, intercalation may open an additional reserve to further enhance and optimize the second-order hyperpolarizabilities without substantial decrease of the energy gap. Based on our recent contribution on intercalation of tripodal push-pull molecule bearing pyridin-4-yl terminus (tris[4-(pyridin-4-yl)phenyl]amine, TPPA),¹¹ we report herein combination of both micro/macrosopic approaches mentioned above. In this respect, three model push-pull molecules with central amino donor and peripheral pyridine acceptor(s) were designed and synthesized. These molecules (4-AminoPYridines, Scheme 1) differ in the number of terminal acceptors and overall molecular arrangement – D- π -A (**APY1**), D-(π -A)₂ (**APY2**), and D-(π -A)₃ (**APY3**). Due to the presence of peripheral basic pyridin-4-yl moieties, the supramolecular arrangement of **APY1-3** can be controlled *via* intercalation into acidic layered inorganic materials. Protonation of the peripheral pyridine rings will generate pyridinium moieties, which are (i) stronger electron acceptors (ICT enhancement), (ii) strongly anchors the whole chromophore between the host layers, and (iii) organizes the dye molecules in bulk (Fig. 1).

Aminopyridines **APY1-3** were intercalated into α -modification of zirconium hydrogen phosphate ($\text{Zr}(\text{HPO}_4)_2 \cdot 2\text{H}_2\text{O}$), zirconium 4-sulfophenylphosphonate $\text{Zr}(\text{HO}_3\text{SC}_6\text{H}_4\text{PO}_3)_2 \cdot 2\text{H}_2\text{O}$ and γ -modification of titanium hydrogen phosphate ($\text{Ti}(\text{PO}_4)(\text{H}_2\text{PO}_4) \cdot 2\text{H}_2\text{O}$). It has recently been verified that commercially available **APY1** undergo intercalation into α -modification of titanium hydrogen phosphate ($\text{Ti}(\text{HPO}_4)_2 \cdot 2\text{H}_2\text{O}$) and generates significant NLO response on condition of its protonation with maleic acid.¹² While **APY2** is increasingly being used for construction of metal-organic frameworks (MOF),¹³ **APY3**, despite it features simple molecular structure, has hypothetically been envisaged as lately as in 2010.¹⁴ To the best of our knowledge, we report herein its first successful preparation. All aminopyridines **APY1-3** and their



Scheme 1 Synthesis of aminopyridines (**APY**) and aminopyridiniums (**MeAPY**).



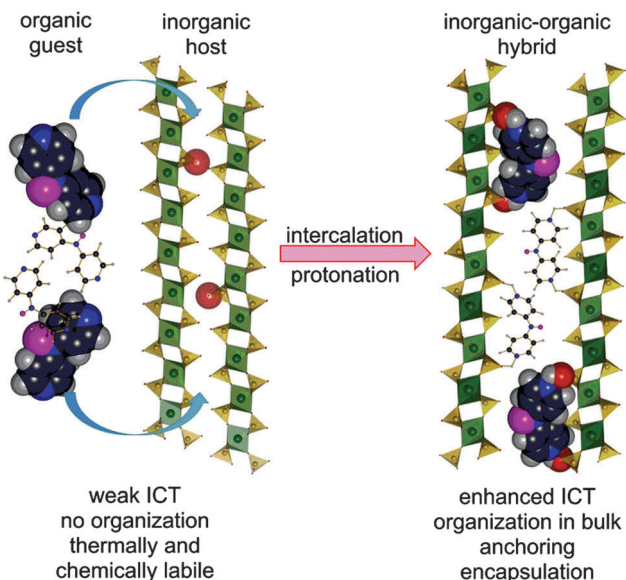


Fig. 1 Schematic representation of the intercalation process of **APY2**.

intercalates were characterized experimentally by X-ray diffraction, TGA, IR, electrochemistry, UV/Vis spectroscopy as well as theoretically by DFT calculations. Their second order susceptibilities (SHG efficiencies) were examined as well.

Results and discussion

Synthesis of aminopyridines

The synthesis of **APY** compounds and their quaternized analogues **MeAPY** is shown in Scheme 1. Dipyridylamine **APY2** was synthesized *via* one-pot pyridine chlorination with PCl_3 and subsequent nucleophilic aromatic substitution with commercially available **APY1**.¹⁵ Introduction of the third pyridine branch was initially attempted *via* Buchwald–Hartwig reaction¹⁶ with 4-iodopyridine yielding no desired product. However, by adopting copper(i)-catalyzed strategy of Sarges *et al.*¹⁷ and upon optimization of the reaction condition, **APY3** was prepared in 47% isolated yield. Electron withdrawing behavior of azines can easily be improved *via* quaternization.¹⁸ Hence, in order to mimic the anticipated products generated upon intercalation into acid layered materials, **APY1–3** were further *N*-methylated with iodomethane to afford pyridinium salts **MeAPY1–3** in almost quantitative yields.

X-ray analysis

Among other spectral characterizations (see the ESI†), the molecular structure of **APY3** was also confirmed by single crystal X-ray analysis. Suitable crystals were obtained by slow evaporation of its methanol solution. The ORTEP plot shown in Fig. 2 confirms the proposed molecular structure of **APY3** and can also be used to determine the extent of the ICT.

In this respect, the involvement of the particular pyridine rings in the ICT can be assessed by their spatial arrangement and bond length alternation (quinoid character δr)¹⁹ and aromaticity

evaluated by Bird index I_6 .²⁰ Central nitrogen atom has perfectly planar environment with three nitrogen atoms of pyridin-4-yl substituents, only N4 atom is slightly shifted out of that central plane. The values of interplanar angles of the central plane and pyridyl rings were found in the narrow region of $37.7\text{--}39.6^\circ$, which is similar to that found for triphenylamine derivatives, *e.g.* TPPA.²¹ The quinoid character and aromaticity of pyridin-4-yl rings were calculated to be within the range of $\delta r = 0.009\text{--}0.010$ and $I_6 = 94.4\text{--}95.9$. Unsubstituted benzene has δr and I_6 equal to 0 and 100, respectively, whereas unsubstituted pyridine has $I_6 = 85.7$. Both indicators imply that all pyridine rings possess relatively low/high quinoid/aromatic character and, thus are involved in less ICT. However, these findings are in accordance with known tripodal triphenylamine derivatives.^{1,11}

Electrochemistry

Electrochemical behaviour of **APY1–3** and **MeAPY1–3** were studied by CV, RDV and polarography. The acquired data are summarized in Table 1. The measured electrochemical behavior of **APY1** is consistent with the data reported in the literature.²² The oxidations of **APY2–3** were not observed in the potential window of the given electrode, electrolyte and solvent (up to $+1.7$ V vs. SCE). The reduction potentials $E_{1/2(\text{red}1)}$ were recorded by polarography. The DME (dropping mercury electrode) allowed a cathodic measurement up to -3 V vs. SCE, while on the Pt-electrode it is only -2 V vs. SCE. Oxidation was observed for pyridinium salts **MeAPY1–3** but this is caused by oxidation of the I^- anions. The first reductions, which are reversible one-electron processes, were measured only with the Pt-electrode as interactions of **MeAPY1–3** with the DME were observed.

When going from **APY2** to **APY3**, the first reduction potentials decrease by 260 mV, most likely as a result of introducing additional electron withdrawing pyridin-4-yl unit. Quaternization of the pyridine to pyridinium moieties significantly shifted the first reduction potentials to more positive values by 0.9 (**APY2** vs. **MeAPY2**) and 1.36 V (**APY3** vs. **MeAPY3**). This clearly reflects the improved electron withdrawing ability and thus enhanced ICT from the central amino donor to peripheral

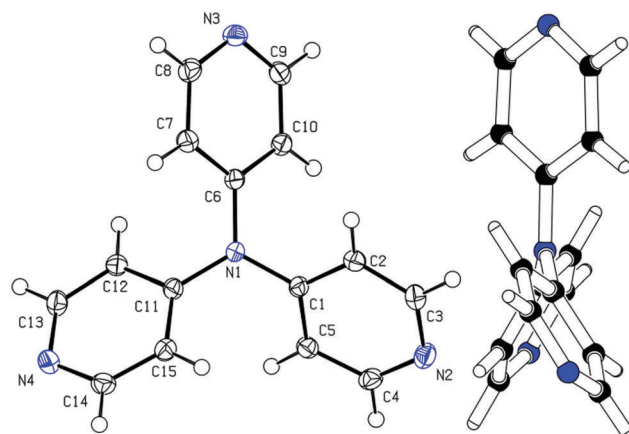


Fig. 2 The molecular structure (ORTEP 50% probability level) and the side view of **APY3**.



Table 1 Experimental and calculated parameters of **APY1–3** and **MeAPY1–3**

Comp.	$E_{1/2(\text{ox1})}^a$ (V)	$E_{1/2(\text{red1})}^a$ (V)	E_{HOMO}^b (eV)	E_{LUMO}^b (eV)	λ_{max}^c (nm(eV))	ε^c (10^3 M cm^{-1})	E_{HOMO}^d (eV)	E_{LUMO}^d (eV)	ΔE^d (eV)	μ^d (D)
APY1	+1.50	—	—	—	267(4.64)sh	1.72	—6.52	—0.66	5.86	5.36
APY2	—	—2.52	—	—1.83	297(4.18)	29.56	—6.35	—1.39	4.95	3.64
APY3	—	—2.26	—	—2.09	302(4.11)	18.43	—6.30	—1.58	4.72	0.02
MeAPY1	—	—1.36	—	—2.99	273(4.54)	17.29	—7.36	—1.96	5.40	0.58
MeAPY2	—	—1.62	—	—2.73	333(3.72)/403(3.08)sh	23.63/22.97	—7.75	—3.21	4.54	0.16
MeAPY3	—	—0.90	—	—3.45	334(3.71)/404(3.07)	30.52/0.62	—7.96	—3.55	4.41	0.06

^a $E_{1/2(\text{ox1})}$ and $E_{1/2(\text{red1})}$ are half-wave potentials of the first oxidation and reduction, respectively. All potentials were recorded in *N,N*-dimethylformamide containing 0.1 M Bu_4NPF_6 and are given vs. SCE. ^b $-E_{\text{HOMO/LUMO}} = E_{1/2(\text{ox1/red1})} + 4.35$ (ref. 23). ^c Measured in DMSO ($c = 2 \times 10^{-5}$ M); sh denotes shoulder. ^d DFT calculated by (B3LYP/6-311++G(2d,p)//B3LYP/6-311++G(2d,p)) in DMF.

pyridinium acceptors. On the contrary, **MeAPY2** was reduced at the most negative potential (−1.62 V) among other pyridinium salts – **MeAPY1** (−1.36 V) and **MeAPY3** (−0.90 V). This is most likely given by a facile loss of HI from **MeAPY2** and formation of an imine structure **MeAPY2q** as shown in the ESI† (Scheme S1). This quinoid cation has also been detected by HR-MALDI-MS as a main peak (Fig. S2, ESI†). In **MeAPY2/MeAPY2q**, the observed most negative reduction potential reflects enhanced electron density of the central amino donor and subsequent higher saturation of the pyridinium acceptor as expressed by the resonant structures shown in Scheme S1 (ESI†).

UV/Vis absorption spectra of **APY1–3** and **MeAPY1–3**

The optical properties of **APY1–3** and **MeAPY1–3** in liquid media were investigated by electronic absorption spectroscopy measured in DMSO (Fig. 3). The measured longest-wavelength absorption maxima λ_{max} and the molar absorption coefficients ε are given in Table 1. All of the absorption spectra, except for **APY1**, are dominated by intense CT-bands with the maxima appearing at 267–302 nm for **APY1–3** and 273–404 nm for **MeAPY1–3**. As expected, these CT-bands are red-shifted with the increasing number of pyridin-4-yl units as well as with their replacement by pyridinium acceptors. **MeAPY2** showed two particularly developed CT-bands appearing at 333 and 403 nm. The latter corresponds to facile formation of the quinoid structure **MeAPY2q** with extended π -conjugated system and stronger electron donor (ICT enhancement). This observation is in accordance with other betaine dyes, especially the Reichardt's dye used to determine the solvent polarity – $E_T(30)$.²⁴ The position of the longest-wavelength absorption maxima and the band-width and shape of betaine dyes are strongly solvent-dependent and methanol seems to be exceptional solvent in this respect.²⁵ Hence, the absorption spectra measured in methanol are shown in the ESI† (Fig. S3). In contrast to DMSO, the spectra of both **MeAPY2** and **3** measured in methanol are dominated by intensive low-energy bands appearing at 390 nm. These pronounced bands can be ascribed to a more efficient ICT from the central amino donor to the peripheral pyridinium acceptors and implies higher stabilization of the formed quinoid structure by protic solvents.

DFT calculations

The spatial and electronic properties of **APY1–3** and **MeAPY1–3** were also investigated by calculations. Their geometry was

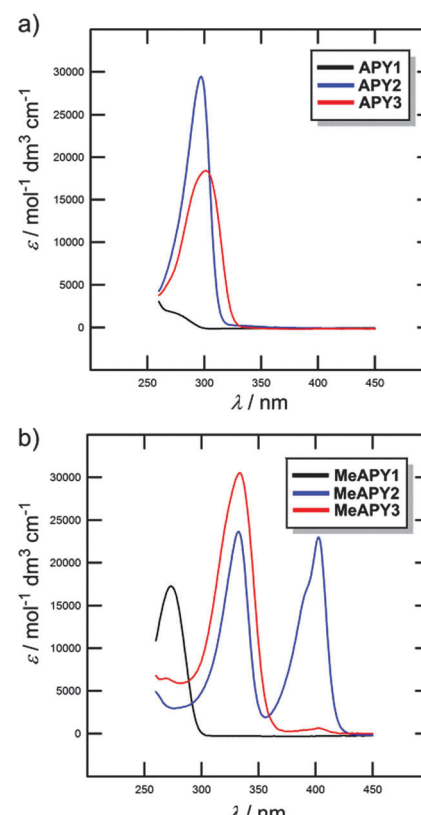


Fig. 3 UV/Vis absorption spectra of **APY1–3** (a) and **MeAPY1–3** (b) measured in DMSO ($c = 2 \times 10^{-5}$ M)

optimized by PM3 and subsequently DFT B3LYP methods with B3LYP/6-311++G(2d,p) basis set. The energies of the highest occupied molecular orbital (HOMO) and lowest unoccupied molecular orbital (LUMO), HOMO–LUMO gap (ΔE), and ground state dipole moment (μ) were calculated by using the B3LYP/6-311++G(2d,p) base, and are summarized in Table 1 (see the ESI† for more details). Only the cationic parts of **MeAPY1–3** were considered in DFT calculations. Although the calculated energies of the LUMO differ slightly from those obtained by electrochemical measurements ($\Delta E_{\text{LUMO}} = 0.1\text{--}1.03$ eV), the DFT-derived HOMO–LUMO gap (ΔE) correlate tightly with the energy of the electron transition calculated from the position of the longest-wavelength absorption maxima ($1240/\lambda_{\text{max}}$) as shown in Fig. S4 (ESI†). Hence, the used DFT calculations are obviously capable of properly describing the trends seen by the



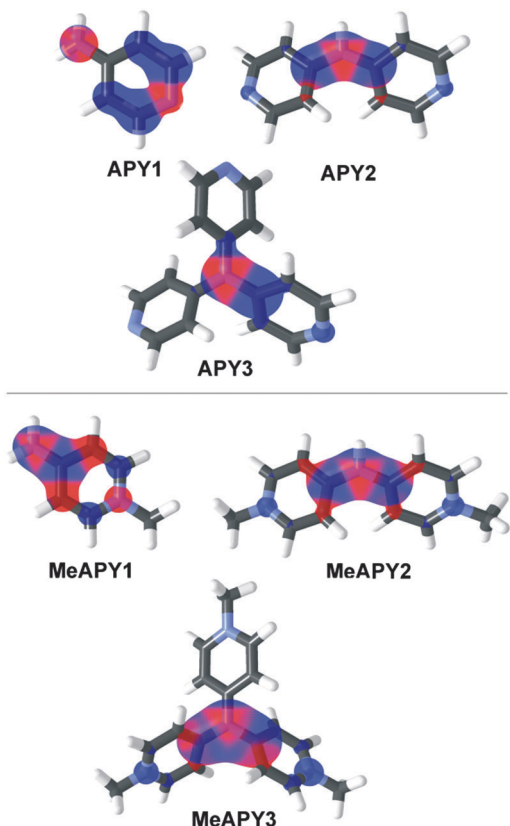


Fig. 4 Optimized geometries and HOMO (red) and LUMO (blue) localizations in **APY1–3** and **MeAPY1–3**.

optical measurements and can be considered as a reasonable tool for the electronic property description of **APY1–3** and **MeAPY1–3**. The principal changes are seen in the energies of the LUMO, which reflects the increasing number of pyridine and pyridinium acceptors appended to the central amino donor. The calculated HOMO–LUMO gaps decrease from 5.86/5.40 to 4.72/4.41 eV for **APY1–3/MeAPY1–3**.

The visualization of frontier molecular orbitals for **APY1–3** and **MeAPY1–3** show acceptor-centered LUMO and donor-centred HOMO, and partial charge separation, which confirms their ICT character (Fig. 4). In tripodal molecules **APY3** and **MeAPY3**, the third pyridin-4-yl branch is occupied by the LUMO+1, the HOMO–1 remained on the central amino donor. This is a common feature of tripodal push–pull molecules.²⁶ As expected, the ground state dipole moment μ vanishes with increasing symmetry of the molecule.

Composition of intercalates

The amount of the intercalate species x in each host is given in Table 2 together with the content of water y . The compositions of the prepared intercalates were calculated on the basis of elemental analysis and thermogravimetric data (thermogravimetry curves are given in Fig. S5–S7 in the ESI†). The general formula can be written as $H \cdot xG \cdot yH_2O$ (where $H = \mathbf{ZrP}$, \mathbf{ZrSPP} , or \mathbf{TiP} and $G = \mathbf{APY1}$, $\mathbf{APY2}$, or $\mathbf{APY3}$). The data in Table 2 shows that the amount of the intercalated guest in the hosts generally

Table 2 Composition of prepared intercalates

Host H	Guest G	Intercalate	x	y
ZrSPP	APY1	ZrSPP-APY1	1.20	0.70
ZrSPP	APY2	ZrSPP-APY2	0.50	1.50
ZrSPP	APY3	ZrSPP-APY3	0.35	1.60
α - ZrP	APY1	ZrP-APY1	0.86	1.00
α - ZrP	APY2	ZrP-APY2	0.43	2.25
α - ZrP	APY3	ZrP-APY3	0.30	1.75
γ - TiP	APY1	TiP-APY1	0.69	1.00
γ - TiP	APY2	TiP-APY2	0.35	0.75
γ - TiP	APY3	TiP-APY3	0.22	2.50

decreases in the order **ZrSPP** > **ZrP** > **TiP**. The ratio of the amount of the intercalated species in each host is roughly the same and is $x_{\mathbf{APY1}} : x_{\mathbf{APY2}} : x_{\mathbf{APY3}} = 6 : 3 : 2$. This ratio is inversely proportional to the charge present at each of the protonated guest species (1 : 2 : 3). The higher amount of the guest in the **ZrSPP** intercalate than in **ZrP** is in accordance with our previous findings for **ZrSPP** and **ZrP** intercalates of tris[4-(pyridin-4-yl)-phenyl]amine.¹¹ There is no distinct relation between the amount of the intercalated guest and the amount of water y .

On heating, all intercalates release water at relatively low temperature, the weight decrease in all cases starts below 100 °C. For the **APY1** intercalates, the second decrease starting at about 300 °C is most probably due to the release of the guest from the interlayer space. Intercalates with **APY2** and **APY3** release their less volatile guests at higher temperature (500 °C) and the decrease corresponding to this release merges with the weight decrease due to the decomposition of the host.

Structure of the host

The intercalation process is driven by acid–base interactions of acidic active sites present on the surface of the host layers with basic guests **APY1–3** (Fig. 1). The intercalation is therefore accompanied by protonation of the peripheral pyridine moieties and generation of pyridinium(s).

All three hosts are layered. All contain acidic active sites, formed by oxygen atoms carrying acid protons. In **ZrP** and **TiP** these active sites are formed by POH groups whereas in **ZrSPP** by SOH groups. The surface density of the active sites on one side of the layer can be expressed as the number of sites per area unit of the layer surface.²⁷ A reciprocal value of the surface density then gives an area available for one active site, which is called ‘free area’. From comparison of the free area with dimension of the intercalated molecule (cross sectional area) we can estimate a maximum amount of the guest which can be intercalated into a given host.

The structure of **ZrSPP** in its inorganic part is based on the structure of the alpha modification of **ZrP**.²⁸ From this it follows that **ZrP** and **ZrSPP** have the same number of active acidic protons per unit of surface that is the same free area on the layer (24 Å²) per active site, that is 48 Å² per formula unit of the host.²⁹

The gamma modification of **TiP** has a different structure.³⁰ Two phosphate groups are present in this gamma modification, one is PO_4^{3-} in which all oxygen atoms are bonded to titanium,



Table 3 Basal spacings d (in Å) of intercalates – an overview

Intercalate	d	d after heating to 210 °C ^a	d after rehydration ^b	Accessible volume (Å ³)
ZrSPP-APY1	24.282	24.14	24.22	359.136
ZrSPP-APY2	23.905	23.61	23.98	341.04
ZrSPP-APY3	26.390	24.80	26.43	460.32
ZrP-APY1	12.653	11.95	12.64	304.944
ZrP-APY2	13.418	11.62	13.58 + 13.36	341.664
ZrP-APY3	12.794	10.92	12.75	311.712
TiP-APY1	15.704	14.52	15.02	213.9816
TiP-APY2	15.156	13.77	15.16	195.9524
TiP-APY3	15.480	14.29	15.45	206.612

^a Measured *in situ* on a heated brass block in the diffractometer. ^b The samples were rehydrated by standing in a closed vessel over water for one week.

the second is H_2PO_4^- with two oxygen atoms bonded to titanium while other two bear acidic protons. The formula of the gamma modification should therefore be written as $\text{Ti}(\text{PO}_4)(\text{H}_2\text{PO}_4)\cdot 2\text{H}_2\text{O}$. The free area surrounding each $\text{P}(\text{OH})_2$ group is 32.9 \AA^2 .³¹

Thickness of the layer defined as the shortest distance between the barycenters of the oxygen atoms situated at the opposite sites of the layer was calculated to be 16.8 \AA , 6.3 \AA , and 9.2 \AA for ZrSPP,²⁸ α -ZrP,³² and γ -TiP,³¹ respectively. By subtraction of these values from the interlayer distances of the intercalates, we can get the height of the gallery available for the incorporation of the intercalated species. When the gallery height is multiplied by the half of the free area (*i.e.*, 24 \AA^2 for ZrSPP and ZrP; 16.5 \AA^2 for TiP) we get the volume which is accessible for the intercalated species in the corresponding host. The corresponding values are given in Table S4 in the ESI.†

Structure of intercalates

The intercalated guest molecules can be placed in the interlayer space in several ways: (i) with the plane of the pyridine rings parallel with the plane of the host layer, either as a one layer of the guest molecules (a “monomolecular” arrangement) or as two layers (a “bimolecular” arrangement); (ii) with the plane of the pyridine ring either perpendicular or tilted with respect to the plane of the host layers. Also in this case the guest molecules can adopt monomolecular or bimolecular arrangement.

The basal spacings/interlayer distances for all intercalates are given in Table 3. In all cases the value of the interlayer distance is increased on intercalation, which indicates that the guest molecules are not placed with the pyridine ring planes parallel to the host layers. In that case the height of the gallery should be about 2 or 4 Å only. With the decrease of amount of the guest in the interlayer space the guest molecule tends to be more inclined with respect to the plane of the host layer.

The gallery height in all APY1 intercalates (7.48 \AA , 6.35 \AA , 6.50 \AA for ZrSPP-APY1, ZrP-APY1 and TiP-APY1, respectively) is larger than or equal to the van der Waals length of the APY1 molecule (6.35 \AA). It means that this molecule can be arranged in the interlayer space with the plane of the pyridine ring perpendicular to the plane of the host layer most probably in an interdigitated manner.

Roughly the same gallery height (7.1 \AA) can be observed for the ZrSPP-APY2 and ZrP-APY2 intercalates while it is much smaller for TiP-APY2 (5.9 \AA). In all cases the gallery height is smaller than the dimension of the APY2 molecule along its longest axis (which is about 10.5 \AA). Therefore, we can rule out the possibility that the guest molecules are bonded to both layers of the host through their pyridinium groups, forming a kind of pillared structure. The more probable arrangement is that in which each guest molecule is bonded to one layer of the host by both pyridinium nitrogen atoms of APY2 as shown in Fig. 1.

High gallery height found for ZrSPP-APY3 (9.6 \AA) indicates that this molecule is in an upright position in ZrSPP, whereas in ZrP and TiP (gallery height 6.5 and 6.3 \AA , respectively) it is tilted with respect to the host layer plane under an estimated angle of 45° .

Change on dehydration

To study the influence of dehydration on the interlayer distance the change of the powder X-ray patterns of the intercalates on heating to 200 \AA was studied. Almost no change of the interlayer distance was observed for ZrSPP-APY1 intercalate, which contains only 0.7 molecule of water per formula unit. In this case the high degree of intercalation ensures quite rigid arrangement of the guest in the interlayer space which does not allow its change on dehydration. Also small decrease of basal spacing (0.3 \AA) was observed for ZrSPP-APY2, even the content of water in this intercalate is higher ($y = 1.5$). The ZrP-APY1 intercalate exhibits a slight decrease of the basal spacing (0.7 \AA), while the decrease for the TiP-APY1 is 1.2 \AA . Both these intercalates contain 1 molecule of water per formula unit and show roughly the same increase of the basal spacing on intercalation (4.3 and 4.5 \AA). The decrease of the basal spacing on dehydration is given by different amount of the intercalated guest. On the other hand, the intercalates of APY3 are most influenced by dehydration, especially ZrP-APY3 (1.9 \AA , $y = 1.75$) and ZrSPP-APY3 (1.6 \AA , $y = 1.6$). Also high decrease of the basal spacing was observed for the ZrP-APY2 intercalate (1.8 \AA) which has the highest amount of water ($y = 2.25$) among all the intercalates.

Infrared spectra

The way how the intercalated guest molecules interact with the host material *i.e.*, the deprotonation of the host and protonation of the guest molecules, was determined on the basis of the IR spectra (see the ESI,† Fig. S8–S16). The peaks in the region from 1150 to 850 cm^{-1} are narrower in the intercalates compared to those in the pristine hosts. The band at 1231 cm^{-1} of $\delta_{\text{P}-\text{OH}}$ found in the spectrum of the original TiP disappears in the spectra of all three TiP intercalates.^{12a} Analogously this band at 1247 cm^{-1} in the spectrum of ZrP disappears in the spectra of ZrP-APY1 and ZrP-APY2; this band is retained in the spectrum of ZrP-APY3, nevertheless, with a lower intensity.

In pure APY1, δ_{NH} scissoring band is observed at 1644 cm^{-1} and peak of ring stretching appears at 1590 , 1558 , 1504 , 1434 cm^{-1} .³³ In this region, a very broad intensive band at



1649 cm^{-1} and quite intensive band at 1535 cm^{-1} are observed in methylated **APY1** (**MeAPY1**). The two bands appear also in the **TiP-APY1** intercalate. In spectra of **ZrSPP-APY1** and **ZrP-APY1** a couple of bands at 1650 and 1675 cm^{-1} and a very broad band at 1540 cm^{-1} are observed. In addition, in the spectrum of **ZrP-APY1** a very weak peak at 1597 cm^{-1} is observed which is observed also in the pristine **APY1**. It indicates that in this intercalate a part of the guest remains unprotonated.

In the spectrum of **ZrSPP-APY2**, the most distinct feature, besides the peaks belonging to the host material, is the existence of peaks at 1624 and 1508 cm^{-1} (see Fig. S9 in the ESI[†]). These peaks are not present in the spectrum of **APY2** but appear in the spectrum of **MeAPY2** at 1654 and 1500 cm^{-1} . In the **ZrP-APY2** intercalate, these peaks appear at 1620 and 1506 cm^{-1} (see Fig. S12 in the ESI[†]) and in **TiP-APY2** at 1626 and 1510 cm^{-1} (Fig. S15 in the ESI[†]). In the case of **ZrSPP-APY3**, the analogous peaks corresponding to methylated (protonated) **APY** are less distinct (Fig. S10 in the ESI[†]). While the positions of these peaks are at 1634 and 1512 cm^{-1} in **MeAPY3**, only a weak peak at 1628 cm^{-1} appears in **ZrSPP-APY3** and the second peak is shifted to 1498 cm^{-1} . In the **ZrP-APY3** intercalate these peaks are more distinct, with the positions at 1628 cm^{-1} and 1500–1508 cm^{-1} , nevertheless, a peak of the host material (**ZrP**) observed at 1614 cm^{-1} might contribute to the intensity of the peak at 1628 cm^{-1} (Fig. S13 in the ESI[†]).

Generally, the IR spectra of the intercalates in the region from 1800 to 1150 cm^{-1} represent a superposition of the peaks found in the host and in the corresponding methylated guest (**MeAPY**). The IR spectra of the intercalates, when compared with the spectra of all three **APY** and **MeAPY**, confirm therefore that these guests are protonated in the intercalates.

Solid state UV/Vis spectra

Beside the measurements in liquid media (see above), the optical properties of **APY1-3**, **MeAPY1-3**, and **APY1-3** intercalates were also investigated in the solid-state (see the ESI[†] Fig. S17–S20).

Unprotonated **APY1** has an absorption maximum (λ_{max}) at 248 nm, whereas methylated **APY1** (**MeAPY1**) showed a maximum at 272 nm. The maxima of all three **APY1** intercalates are roughly at the same position, around 260 nm (Fig. S18, ESI[†]). The **ZrSPP-APY1** intercalate showed slightly bathochromically shifted λ_{max} at 262 nm, which reflects that **ZrSPP** is a host material with the strongest acidity of the interlayer environment among all three hosts. **APY1** protonated by the exposition of this compound to HCl vapours shows a maximum at around 265 nm and its spectrum is similar to those of all three intercalates.

Significant changes in the UV/Vis spectra were observed when going from **APY2** to methylated **MeAPY2**. Whereas unprotonated **APY2** showed a single peak at 293 nm, **MeAPY2** possesses two maxima at 326 and at 392 nm. This is similar to that observed by measurement in DMSO (see above). Compared to the **APY1** intercalates, the difference between the spectra of all three **APY2** intercalates is clearly distinguishable (Fig. S19, ESI[†]). The **ZrP-APY2** intercalate has the maximum at the lowest wavelength (297 nm) almost at the same position as the unprotonated **APY2**

guest, with a shoulder at around 320–330 nm. This means that in **ZrP-APY2** we can distinguish between the unprotonated and protonated forms of **APY2**. This claim is further supported by the fact that **APY2** protonated in HCl vapours has a maximum at 321 nm, which is the same region as found for the shoulder in the **ZrP-APY2** spectrum. The **TiP-APY2** and **ZrSPP-APY2** intercalates showed one envelope band with the maxima at 305 and 317 nm, respectively. These bands seem to be superposition of that found for **APY2** and its protonated form. From these data we can deduce that **APY2** undergoes partial protonation during intercalation into all three hosts and is being most protonated in **ZrSPP** (most bathochromically shifted maxima). Thus, the acidity of the hosts increases in the order **ZrP** < **TiP** < **ZrSPP**.

In the solid-state, **APY3** and **MeAPY3** showed the UV/Vis spectra similar to those observed in methanol (see above) with the maxima appearing at 307 and 323/390 nm, respectively. The **ZrP-APY3** intercalate possesses almost the same maximum as **APY3** with a shoulder at around 325 nm (Fig. S20, ESI[†]). The spectrum of the **TiP-APY3** intercalate shows a very broad unstructured band covering the range of 300–320 nm with the maximum reaching the position observed for **APY3** exposed to HCl vapors ($\lambda_{\text{max}} = 324$ nm). The longest-wavelength absorption maximum of **ZrSPP-APY3** ($\lambda_{\text{max}} = 323$ nm) corresponds tightly to the maximum measured for protonated **APY3**, but in contrast to **MeAPY3**, shows no shoulder. This implies that **APY3** intercalated into **ZrSPP** is fully protonated.

NLO properties

To create a long-range ordered non-centrosymmetry the investigated chromophores were embedded into liquid photocomposition of oligoetheracrylate photopolymers,³⁴ which were photo-solidified by nitrogen 337 nm cw laser with power density 55 W cm^{-2} at an applied electric field successively increasing up to 4 kV cm. The orientation control was done using a polarized absorption. Typical time kinetics of the fundamental and the SHG signals is shown in the ESI[†] (Fig. S21). The measured principal second-order susceptibility parameters d_{eff} jointly with the calculated hyperpolarizabilities $\beta(-2\omega; \omega, \omega)$ of **APY1-3**, **MeAPY1-3** and intercalates are listed in Table 4.

The NLO data in Table 4 allows evaluation of the structure–property relationships caused by the chromophore arrangement, *N*-methylation as well as intercalation. The effect of the chromophore arrangement can easily be assessed on the series **APY1-3**. The linear push–pull aminopyridine **APY1** showed a SHG response with d_{eff} equal to 1.34 pm V^{−1}. An introduction of the second pyridin-4-yl branch as in **APY2** increased the second-order susceptibility to 1.56 pm V^{−1}. On the contrary, tripodal **APY3** showed a significantly diminished NLO response with $d_{\text{eff}} = 0.35$ pm V^{−1}. This drop reflects the symmetrical arrangement of **APY3** (see the X-ray analysis above) and the very low calculated ground-state dipole moment (Table 1). The extent of the ICT and resulting NLO properties of the heteroaromatic D–π–A systems can be improved *via* alkylation. Thus, the comparison of **MeAPY1-3** *vs.* **APY1-3** allows evaluation of the effect of the pyridine/pyridinium acceptors. Whereas, the pairs of corresponding chromophores **MeAPY1/APY1** and **MeAPY2/APY2**



Table 4 Second-order susceptibilities and DFT calculated hyperpolarizabilities of **APY1–3**, **MeAPY1–3**, and intercalates

Comp.	d_{eff}^a (pm V ⁻¹)	$\beta^b (-2\omega; \omega, \omega)$ (10 ⁻³⁰ esu)
APY1	1.34	1.06
APY2	1.56	1.44
APY3	0.35	0.01
MeAPY1	1.42	1.37
MeAPY2	1.67	2.61
MeAPY3	1.04	0.13
ZrSPP-APY1	1.78	—
ZrSPP-APY2	1.89	—
ZrSPP-APY3	1.21	—
ZrP-APY1	1.67	—
ZrP-APY2	1.72	—
ZrP-APY3	1.45	—
TiP-APY1	2.01	—
TiP-APY2	2.21	—
TiP-APY3	1.56	—

^a Measured in oligoetheracrylate at 1064 (± 0.15 pm V⁻¹). ^b DFT calculated by (B3LYP/6-311+G(2d,p)//B3LYP/6-311+G(2d,p)) in vacuum at 1064 nm.

showed slightly improved nonlinearities by a factor of 1.06/1.07, the nonlinearity of **MeAPY3** is almost three times higher than that found for **APY3**. This observation is most likely given by a synergistic effect of the ICT enhancement *via* *N*-methylation and the symmetry loss caused by iodide counter ions. In general, the SHG response of aminopyridines decreases in the order of **APY2** > **APY1** > **APY3** and **MeAPY2** > **MeAPY1** > **MeAPY3** and **MeAPY** > **APY**. The calculated hyperpolarizabilities $\beta(-2\omega; \omega, \omega)$ showed very similar trends.

The intercalation of **APY1–3** into **ZrSPP**, **ZrP**, and **TiP** is accompanied by their protonation as well organization in the bulk. Whereas the effect of protonation can be considered similar to quaternization, the significant SHG improvement seen for all intercalates over **MeAPY1–3** must be elucidated as the impact of their organization in the layered host. The measured SHG responses reflect the acidity of the host, where intercalates with the most acidic **ZrSPP** showed larger d_{eff} than **ZrP** (except **APY3**). The highest nonlinearities were measured for **APY1–3** intercalated into gamma modification of titanium hydrogen phosphate (**TiP**). In the **TiP** intercalates, the lowest volume left in the interlayer space of the host after intercalation of **APY1–3** were found. This can be expressed as the lowest difference between the accessible volume in the interlayer space of the host V_H and the volume of the intercalated molecule V_{guest} and is documented in Table S4 in the ESI[†] together with the corresponding calculations. Thus, the arrangement of the guest molecules in **TiP** turned out to be the most rigid among all three hosts. In agreement with our assumptions given in the Introduction this reduced internal motion of the guests leads to an increased NLO response.

Conclusions

A series of model organic push–pull aminopyridines with various spatial arrangements has been synthesized to examine their intercalation into inorganic layered materials (alpha modification of

zirconium hydrogen phosphate, zirconium 4-sulfophenylphosphonate, and gamma modification of titanium hydrogen phosphate). The prepared inorganic–organic hybrids were further investigated as ordered materials for nonlinear optics.

A facile synthetic pathway has been developed to novel tripodal tris(pyridin-4-yl)amine (**APY3**). Its structure was unambiguously confirmed by single crystal X-ray analysis, which revealed almost perfectly planar environment of all three peripheral nitrogen atoms. The fundamental properties of all push–pull aminopyridines were investigated by electrochemistry, UV/Vis absorption spectra and were completed with DFT calculations. It was demonstrated that with increased number of the pyridin-4-yl acceptor units, the HOMO–LUMO gap decreases steadily by more than 1 eV and the longest-wavelength absorption maxima shifts bathochromically ($\Delta\lambda_{\text{max}} \sim 30$ nm). *N*-Quaternization, which takes place exclusively on the peripheral pyridines, caused further reduction of the HOMO–LUMO gap and red-shifts the CT-band. Structural analysis of **MeAPY** compounds revealed facile formation of the quinoid structures, which significantly affected their electrochemical and optical properties.

Three types of intercalates were prepared with the ratio of the amount of intercalated **APY1–3** molecules being 6:3:2. This ratio is inversely proportional to the charge generated at each of the aminopyridine guest (1:2:3). IR and solid-state UV/Vis spectra showed that all aminopyridines underwent protonation during the intercalation process, which extent depends on the number of guest basic centers as well as acidity of the host. Taking spectra of **APY1–3** and **MeAPY1–3** as limiting, the measured IR spectra of the intercalates are superposition of the peaks found for the host and methylated guest. This observation confirms intercalation process as well as guest protonation. From the UV/Vis spectra, the extent of the protonation can further be assessed. Whereas **APY2** underwent only partial protonation upon intercalation, full protonation of **APY3** was observed in the most acidic **ZrSPP** and **TiP** hosts. Powder X-ray diffraction measurements revealed that the guest molecules are arranged in the interlayer space of the hosts as interdigitated monolayers in the way schematically shown in Fig. 1 for **APY2** intercalated in **ZrP**. In view of a generally low thermal stability of organic push–pull molecules, the prepared inorganic–organic materials resisted thermal decomposition up to 300 (**APY1**) and 500 °C (**APY2–3**). This feature makes them thermally very robust.

Second-order nonlinear optical properties of **APY1–3**, quaternized **MeAPY1–3**, and **APY1–3** intercalates were examined by SHG. The measured as well as calculated optical susceptibilities/hyperpolarizabilities were affected by the following structural features:

- arrangement of the push–pull aminopyridine (a general decrease in the SHG response was observed in the order of **APY2** > **APY1** > **APY3**)
- quaternization/protonation (pyridine *vs.* pyridinium acceptor moieties, ICT enhancement)
- intercalation into layered materials (all intercalates showed significantly higher SHG responses than pure organic push–pull guests)
- acidity of the host material used for intercalation (**ZrSPP** and **TiP** proved to be more efficient acids than **ZrP**)

• structure of the host (compared to **ZrSPP** and **ZrP**, the **TiP** intercalates have more tightly arranged **APY** molecules and showed higher SHG response).

In this work, we have verified a new strategy on property tuning of organic push-pull molecules. Three aminopyridines with D- π -A, D-(π -A)₂, and D-(π -A)₃ arrangements were designed, synthesized, and investigated as model guest molecules capable of intercalation into inorganic layered materials providing access to new inorganic-organic hybrid materials. We believe that this multidisciplinary study would serve as useful guide in designing novel NLO-active materials with tailored properties.

Experimental

Aminopyridines

APY1 is commercially available; the synthesis of **APY2** and **APY3** is outlined in Scheme 1 and described in the ESI.[†]

Intercalates

Three layered host materials were used for the intercalation, namely alpha modification of zirconium hydrogen phosphate with formula $\text{Zr}(\text{HPO}_4)_2 \cdot \text{H}_2\text{O}$ (denoted further as **ZrP**), zirconium 4-sulfophenylphosphonate with formula $\text{Zr}(\text{HO}_3\text{SC}_6\text{H}_4\text{PO}_3)_{1.8} \cdot (\text{C}_6\text{H}_5\text{PO}_3)_{0.2} \cdot 2\text{H}_2\text{O}$ (**ZrSPP**) and gamma modification of titanium hydrogen phosphate with formula $\text{Ti}(\text{PO}_4)(\text{H}_2\text{PO}_4) \cdot 2\text{H}_2\text{O}$ (**TiP**). The syntheses of the host materials (**ZrP**, **ZrSPP** and **TiP**) and the intercalation of **APY1**, **APY2** and **APY3** into them are described in the ESI.[†]

Materials and methods

Reagents and solvents were reagent grade and were used as received. ¹H and ¹³C NMR spectra were recorded at 500 and 125 MHz, with a Bruker AVANCE 500 instruments at 25 °C equipped with Prodigy CryoProbe. High resolution MALDI MS spectra were measured on a MALDI mass spectrometer LTQ Orbitrap XL (Thermo Fisher Scientific, Bremen, Germany) equipped with nitrogen UV laser (337 nm, 60 Hz). Elemental analyses were performed on an EA 1108 Fisons instrument. UV/Vis spectra were recorded on a Hewlett-Packard 8453 spectrophotometer. Electrochemical measurements were carried out in *N,N*-dimethylformamide containing 0.1 M Bu_4NPF_6 in a three electrode cell by cyclic voltammetry (CV), rotating disk voltammetry (RDV) and polarography. The working electrode was platinum disk (2 mm in diameter) for CV and RDV experiments. As the reference and auxiliary electrodes were used saturated calomel electrode (SCE) separated by a bridge filled with supporting electrolyte and Pt wire, respectively. All potentials are given *vs.* SCE. Voltammetric measurements were performed using a potentiostat PGSTAT 128N (AUTOLAB, Metrohm Autolab B.V., Utrecht, The Netherlands) operated *via* NOVA 1.10 software. The X-ray data for the crystals of **APY3** were obtained at 150 K using an Oxford Cryostream low-temperature device on a Nonius KappaCCD diffractometer

with Mo K α radiation ($\lambda = 0.71073 \text{ \AA}$), a graphite monochromator, and the ϕ and χ scan mode.

Powder X-ray diffraction data were obtained with a D8 Advance diffractometer (Bruker AXS, Germany) with Bragg-Brentano θ - θ geometry (40 kV, 30 mA) using CuK α radiation with secondary graphite monochromator. The diffraction angles were measured at room temperature from 2 to 70° (2 θ) in 0.02° steps with a counting time of 15 s per step. Powder X-ray diffraction measurements at 210 ± 1 °C were carried out on a heated brass block equipped with a thermocouple in the range from 2 to 35° (2 θ) in 0.025° steps with a counting time of 15 s per step. The size of the crystallites of the intercalates was calculated according to the Scherrer formula³⁵ using an EVA software.³⁶

The thermogravimetric measurements (TGA) were done using a home-made apparatus constructed of a computer-controlled oven and a Sartorius BP210 S balance. The measurements were carried in air between 30 and 960 °C at a heating rate of 5 °C min⁻¹.

Infrared spectra in the range of 600–4000 cm⁻¹ were recorded at 64 scans per spectrum at 2 cm⁻¹ resolution using HATR adapter on a Perkin-Elmer FTIR Spectrum BX spectrometer on neat samples. All spectra were corrected for the presence of moisture and carbon dioxide in the optical path.

Second-order non-linear optical susceptibilities were measured by a method similar to that described in the ref. 37 where a polymer supported the crystalline powder. The pulsed Q-switch Nd:YAG laser operating at 1064 nm wavelength with a pulse duration of 18 ns and frequency repetition 10 Hz, power about 1 MW and a pulse repetition about 10 Hz was applied as the fundamental one. The samples were rotated on the travel in order to achieve a maximal SHG which was spectrally separated by a monochromator connected to photomultiplier. The optimal content of chromophore was equal to about 30% in weighting units. LiNbO₃ crystals with known parameters of a second-order optical susceptibility were used as reference samples. Using the ratio of the intensities for the reference and the studied samples we have defined the second order susceptibilities with accuracy up to 0.15 pm V⁻¹.

Acknowledgements

This work has been supported by the Czech Science Foundation (13-01061S).

Notes and references

- (a) F. Bureš, *RSC Adv.*, 2014, **4**, 58826; (b) M. Kivala and F. Diederich, *Acc. Chem. Res.*, 2009, **42**, 235; (c) H. Meier, *Angew. Chem., Int. Ed.*, 2005, **44**, 2482.
- (a) J. M. Hales, S. Barlow, H. Kim, S. Mukhopadhyay, J.-L. Brédas, J. W. Perry and S. R. Marder, *Chem. Mater.*, 2014, **26**, 549; (b) P. N. Prasad and D. J. Williams, *Introduction to Nonlinear Optical Effects in Molecules & Polymers*, John Wiley & Sons, New York, 1991; (c) D. R. Kanis, M. A. Ratner and



T. J. Marks, *Chem. Rev.*, 1994, **94**, 195; (d) J. J. Wolff and R. Wortmann, *Adv. Phys. Org. Chem.*, 1999, **32**, 121; (e) G. S. He, L.-S. Tan, Q. Zheng and P. N. Prasad, *Chem. Rev.*, 2008, **108**, 1245.

3 M. G. Kuzyk, *J. Mater. Chem.*, 2009, **19**, 7444.

4 (a) M. G. Kuzyk, *Phys. Rev. Lett.*, 2000, **85**, 1218; (b) M. G. Kuzyk, *J. Chem. Phys.*, 2006, **125**, 154108; (c) J. Pérez Moreno and M. G. Kuzyk, *J. Chem. Phys.*, 2005, **123**, 194101.

5 M. G. Kuzyk, C. W. Dirk and C. W. Characterization Techniques and *Tabulations for Organic Nonlinear Optical Materials*, Marcel Dekker, New York, 1998.

6 (a) L. R. Dalton, *J. Phys.: Condens. Matter*, 2003, **15**, R897; (b) M. J. Cho, D. H. Choi, P. A. Sullivan, A. J. P. Akelaitis and L. R. Dalton, *Prog. Polym. Sci.*, 2008, **33**, 1013; (c) J. Luo, X.-H. Zhou and A. K.-Y. Jen, *J. Mater. Chem.*, 2009, **19**, 7410; (d) L. R. Dalton, P. A. Sullivan and D. H. Bale, *Chem. Rev.*, 2010, **110**, 25.

7 (a) N. Epelde-Elezcano, E. Duque-Redondo, V. Martínez-Martínez and H. Manzano, *Langmuir*, 2014, **30**, 10112; (b) M. Ogawa, M. Takahashi and K. Kuroda, *Chem. Mater.*, 1994, **6**, 715; (c) M. Ogawa and A. Ishikawa, *J. Mater. Chem.*, 1998, **8**, 463; (d) G. G. Aloisi, U. Costantino, F. Elisei, L. Latterini, C. Natali and M. Nocchetti, *J. Mater. Chem.*, 2002, **12**, 3316; (e) R. Takenawa, Y. Komori, S. Hayashi, J. Kawamata and K. Kuroda, *Chem. Mater.*, 2001, **13**, 3741.

8 U. Díaz, Á. Cantín and A. Corma, *Chem. Mater.*, 2007, **19**, 3686.

9 (a) J. S. O. Evans, S. Bénard, P. Yu and R. Clément, *Chem. Mater.*, 2001, **13**, 3813; (b) S. Bénard, A. Léaustic, E. Rivière, P. Yu and R. Clément, *Chem. Mater.*, 2001, **13**, 3709; (c) T. Coradin, R. Clément, P. G. Lacroix and K. Nakatani, *Chem. Mater.*, 1996, **8**, 2153.

10 (a) Y. Suzuki, Y. Tenma, Y. Nishioka and J. Kawamata, *Chem. - Asian J.*, 2012, **7**, 1170; (b) L. Latterini, M. Nocchetti, G. G. Aloisi, U. Costantino and F. Elisei, *Inorg. Chim. Acta*, 2007, **360**, 728; (c) M. Ogawa and K. Kuroda, *Chem. Rev.*, 1995, **95**, 399.

11 K. Melánová, D. Cvejn, F. Bureš, V. Zima, J. Svoboda, L. Beneš, T. Mikysek, O. Pytela and P. Knotek, *Dalton Trans.*, 2014, **43**, 10462.

12 (a) L. M. Nunes and C. Airoldi, *Thermochim. Acta*, 2005, **435**, 118; (b) J. Tarasiewicz, R. Jakubas, I. Majerz, J. Baran, A. Gągor and A. Miniewicz, *Vib. Spectrosc.*, 2013, **66**, 93.

13 (a) R. L. LaDuca, R. Finn and J. Zubieta, *Chem. Commun.*, 1999, 1669; (b) S. M. Saylor, R. M. Supkowski and R. L. LaDuca, *Inorg. Chim. Acta*, 2008, **361**, 317; (c) S. H. Qiblawi, L. K. Sposato and R. L. LaDuca, *Inorg. Chim. Acta*, 2013, **407**, 297; (d) M.-L. Han, Y.-P. Wu, J. Zhao, D.-S. Li and Y.-Y. Wang, *J. Solid State Chem.*, 2015, **230**, 218; (e) L. E. Weingartz, J. H. Nettleman, G. A. Farnun, R. J. Staples and R. L. LaDuca, *Polyhedron*, 2015, **89**, 168.

14 Y. G. Bushuev and G. Sastre, *J. Phys. Chem. C*, 2010, **114**, 19157.

15 (a) E. Koenigs and G. Jung, *J. Prakt. Chem.*, 1933, **137**, 141; (b) R. S. Alekseev, A. V. Kurkin and M. A. Yurovskaya, *Chem. Heterocycl. Compd.*, 2012, **48**, 1235.

16 B. P. Fors, P. Krattiger, E. Strieter and S. L. Buchwald, *Org. Lett.*, 2008, **10**, 3505.

17 R. Sarges, H. R. Howard, K. M. Donahue, W. M. Welch, B. W. Dominy, A. Weissman, B. K. Koe and J. Bordner, *J. Med. Chem.*, 1986, **29**, 8.

18 (a) E. Cariati, R. Macchi, D. Roberto, R. Ugo, S. Galli, N. Masciocchi and A. Sironi, *Chem. Mater.*, 2007, **19**, 3704; (b) T. Cañeque, A. M. Cuadro, J. Alvarez-Builla, J. Pérez-Moreno, K. Clays, G. Marcelo, F. Mendicuti, O. Castaño, J. L. Andrés and J. J. Vaquero, *Eur. J. Org. Chem.*, 2010, 6323; (c) M. A. Ramirez, R. Custodio, A. M. Cuadro, J. Alvarez-Builla, K. Clays, I. Asselberghs, F. Mendicuti, O. Castaño, J. L. Andrés and J. J. Vaquero, *Org. Biomol. Chem.*, 2013, **11**, 7145.

19 C. Dehu, F. Meyers and J. L. Brédas, *J. Am. Chem. Soc.*, 1993, **115**, 6198.

20 (a) C. W. Bird, *Tetrahedron*, 1986, **42**, 89; (b) S. I. Kotelevskii and O. V. Prezhdo, *Tetrahedron*, 2001, **57**, 5715; (c) T. M. Krygowski, H. Szatylowicz, O. A. Stasyuk, J. Dominikowska and M. Palusiak, *Chem. Rev.*, 2014, **114**, 6383.

21 (a) C. Hua, P. Turner and D. M. D'Alessandro, *Dalton Trans.*, 2013, **42**, 6310; (b) M.-D. Zhang, C.-M. Di, L. Qin, X.-Q. Yao, Y.-Z. Li, Z.-J. Guo and H.-G. Zheng, *Cryst. Growth Des.*, 2012, **12**, 3957.

22 (a) I. B. Romanova and L. V. Chervina, *Chem. Heterocycl. Compd.*, 1977, **13**, 1321; (b) P. G. Desideri, D. Heimler and L. Lepri, *J. Electroanal. Chem.*, 1978, **87**, 275.

23 A. A. Isse and A. Gennaro, *J. Phys. Chem. B*, 2010, **114**, 7894.

24 (a) C. Reichardt, *Solvents and Solvent Effects in Organic Chemistry*, Second, completely revised and enlarged edition, VCH, Weinheim, 1988; (b) C. Reichardt, *Angew. Chem.*, 1965, **77**, 30.

25 A. M. Kjaer and J. Ulstrup, *J. Am. Chem. Soc.*, 1987, **109**, 1934.

26 D. Cvejn, E. Michail, I. Polyzos, N. Almonasy, O. Pytela, M. Klikar, T. Mikysek, V. Giannetas, M. Fakis and F. Bureš, *J. Mater. Chem. C*, 2015, **3**, 7345.

27 G. Alberti and U. Costantino, Layered Solids and their intercalation chemistry, in *Comprehensive Supramolecular Chemistry. Two- and Three-dimensional networks*, ed. J. L. Atwood, 1996, vol. 7, pp. 1–23.

28 J. Svoboda, V. Zima, K. Melánová, L. Beneš and M. Trchová, *J. Solid State Chem.*, 2013, **208**, 58.

29 A. Clearfield and U. Costantino, Layered metal phosphates and their intercalation chemistry, in *Comprehensive Supramolecular Chemistry*, ed. G. Alberti and T. Bein, Pergamon Press, Oxford, 1996, vol. 7, pp. 107–149.

30 A. N. Christensen, E. K. Andersen, I. G. K. Andersen, G. Alberti, M. Nielsen and M. S. Lehmann, *Acta Chem. Scand.*, 1990, **44**, 865.

31 G. Alberti, Layered metal phosphates and their intercalation chemistry, in *Comprehensive Supramolecular Chemistry*, ed. G. Alberti and T. Bein, Pergamon Press, Oxford, 1996, vol. 7, pp. 142.



32 A. Clearfield and U. Costantino, Layered metal phosphates and their intercalation chemistry, in *Comprehensive Supramolecular Chemistry*, ed. G. Alberti and T. Bein, Pergamon, New York, 1996, vol. 7, p. 113.

33 Y. Buyukmurat and S. Akyuz, *J. Mol. Struct.*, 2003, **651**–653, 533.

34 B. Sahraoui, I. V. Kityk, J. Bieleninik, P. Hudhomme and A. Gorgues, *Mater. Lett.*, 1999, **41**, 164.

35 A. Patterson, *Phys. Rev.*, 1939, **56**, 978.

36 EVA, ver.19., Diffrac plus Basic Evaluating Package, Bruker AXS GmbH, Germany, 2013.

37 S. K. Kurtz and T. T. Perry, *J. Appl. Phys.*, 1968, **39**, 3798.

